

# Diffusion-Based Feature Denoising and Using NNMF for Robust Brain Tumor Classification

Hiba Adil Al-kharsan <sup>1</sup>, Róbert Rajkó <sup>2,3\*</sup>

<sup>1</sup> Doctoral School of Computer Science, University of Szeged, Árpád tér 2, H-6720 Szeged, Hungary; hibaadil@inf.u-szeged.hu

<sup>2</sup> University Research and Innovation Center (EKIK), Óbuda University, Bécsi út 96/b, H-1034 Budapest, Hungary; rajko.robert@uni-obuda.hu

<sup>3</sup> Academic Staff, Doctoral School of Computer Science, University of Szeged, Árpád tér 2, H-6720 Szeged, Hungary; rajko@sol.cc.u-szeged.hu

\* Correspondence: rajko.robert@uni-obuda.hu; EKIK OE

## Abstract

Brain tumor classification from magnetic resonance imaging, which is also known as MRI, plays a sensitive role in computer-assisted diagnosis systems. In recent years, deep learning models have achieved high classification accuracy. However, their sensitivity to adversarial perturbations has become an important reliability concern in medical applications. This study suggests a robust brain tumor classification framework that combines Non-Negative Matrix Factorization (NNMF or NMF), lightweight convolutional neural networks (CNNs), and diffusion-based feature purification. Initially, MRI images are preprocessed and converted into a non-negative data matrix, from which compact and interpretable NNMF feature representations are extracted. Statistical metrics, including AUC, Cohen's d, and p-values, are used to rank and choose the most discriminative components. Then, a lightweight CNN classifier is trained directly on the selected feature groups. To improve adversarial robustness, a diffusion-based feature-space purification module is introduced. A forward noise method followed by a learned denoiser network is used before classification. System performance is estimated using both clean accuracy and robust accuracy under powerful adversarial attacks created by AutoAttack. The experimental results show that the proposed framework achieves competitive classification performance while significantly enhancing robustness against adversarial perturbations. The findings presuppose that combining interpretable NNMF-based representations with a lightweight deep approach and diffusion-based defense technique supplies an effective and reliable solution for medical image classification under adversarial conditions.

**Keywords:** Brain Tumor Classification; Non-Negative Matrix Factorization (NNMF); Diffusion-Based Defense; AutoAttack+ (AA+); Metrics for Classification Models; CNN-based Classification

## 1. Introduction

The classification of brain tumors from magnetic resonance imaging (MRI) is a large and complex component in computer-supported diagnostic systems. Early and careful detection improves handling, design, and patient survival. In recent years, deep learning approaches, mostly convolutional neural networks (CNNs), have shown remarkable performance in the medical image analysis job [1]. CNN-based models have high classification accuracy in brain tumor detection and segmentation problems due to their ability to learn hierarchical features directly from data.

Despite their powerful predictive performance, deep neural networks are highly vulnerable to adversarial attacks. Little, carefully crafted input modifications can safely degrade classification accuracy while remaining visually imperceptible [2]. This sensitivity raised serious concerns in safety-critical applications, such as medical diagnosis, where solidity and robustness are essential. To ensure a robust evaluation of the robustness of the framework, united attack benchmarks such as AutoAttack have been suggested [3].

Feature extraction [4] and dimensionality reduction remain key components for building interpretable and computationally efficient classification models. Similar chemometric approaches such as PLS-DA have been successfully applied in other domains, illustrating the value of interpretable low-dimensional representations. [5]. Non-negative matrix factorization (NNMF or NMF) is a well-confirmed method to decompose non-negative data into representations based on collective parts [6]. Unlike unconstrained linear techniques such as Principal Component Analysis (PCA), NNMF step non-negativity bands, resulting in an interpretable low-rank string. This property makes NNMF especially suitable for medical image analysis, where the pixel density and derived features are inherently non-negative [7].

In this work, we suggest a structured framework for brain tumor classification that combines NNMF-based feature extraction, statistical feature ranking, CNN-based classification, and diffusion-based feature purification for adversarial robustness. Firstly, MRI images are converted into non-negative feature matrices and decomposed using NNMF. The extracted components are statistically evaluated using metrics such as Area Under the Curve (AUC), Cohen's  $d$ , and hypothesis testing to identify the most spatial features. Then, a lightweight CNN classifier is trained on the selected feature subset. To improve robustness, a feature-space diffusion is introduced to affect structured noise injection, followed by a learned denoising network that borders the reverse diffusion operation. System performance is evaluated against strong adversarial attacks using AutoAttack [3], with the implementation adopted from the official public store [8]. The estimate compares baseline and defended models in terms of both clean precision and robust precision. The suggested path demonstrates that the combination of interpretable NNMF representations with lightweight deep models and diffusion-based purification provides competitive classification accuracy while improving robustness versus adversarial trouble.

## 2. Related Works

- Brain Tumor Detection Using CNN

Hossain et al. [9] suggest a hybrid brain tumor detection framework that joins classical machine learning classifiers with a computational neural network (CNN). The research used the BRATS benchmark dataset and applied Fuzzy C-Means (FCM) clustering for tumor segmentation, followed by feature extraction using texture and statistical descriptors.

In the classical machine learning phases, several classifiers were evaluated, including Support Vector Machine (SVM), K-Nearest Neighbors (KNN), Logistic Regression, Naïve Bayes, Random Forest and Multilayer Perception (MLP). between them, SVM achieved the best performance with an accuracy of 92.42%.

For deep learning-based classification, the researcher designed a five-layer CNN structure depending on convolution, max-pooling, flattening, and fully linked layers. The suggested CNN achieved 97.87% accuracy in an 80:20 training–testing split, outperforming traditional classifiers. However, the performance reported increases; the approach relies on pixel-level segmentation and explicit image-based CNN classification. In contrast, our work achieves interpretable low-rank NNMF representations combined with a lightweight CNN approach and diffusion-based robustness boost, aiming not only at high classification accuracy but also improved adversarial robustness.

- NMF-CNN for the enhancement of features

Chan et al. [10] suggest a hybrid NMF-convolutional neural network (NMF-CNN) framework for the detection of sound events in the DCASE 2019 challenge. In their work, NMF was used as a preprocessing and feature enhancement step to approximate powerful labels from weakly labeled data by resolving the analysis matrix  $H$ . The extracted representations were then fed into a CNN approach for event classification. The results of their study showed that the integration of NMF with a shallow CNN enhances the event-based F1-score (30.39%) compared to the baseline system (23.7%), explaining that NMF can provide a meaningful structural decay that benefits

deep learning architectures. Unlike their system in voiced scene analysis, the current study adopts NNMF for medical image feature extraction, where it is applied to generate interpretable low-rank representations of brain MRI images. Subsequently, these representations are utilized for classification and robustness evaluation under autoattacks

- **Semi-NMF Network for Image Classification**  
Huang et al. [11] suggest a Semi-NMF-based convolutional network (SNnet) for image classification, where Convolutional filters are not learned through backpropagation but instead are built using semi-non-negative matrix factorization used to image patches. Unlike traditional CNNs that depend on slope-based optimization, Their process learns filter banks by matrix factorization, reduces computational value, and avoids global parameter tuning. In addition, a weakly supervised extension (S-SNnet) was introduced via merge graph regularization into the Semi-NMF framework to enhance discriminative capability. Experimental results on the MNIST dataset demonstrated that The suggested style achieves competitive performance compared to state-of-the-art shallow and deep learning architectures such as PCANet. This work highlights the feasibility of merging the matrix factorization mechanism within convolutional frameworks for active feature learning.
- **Classification-Denoising Joint Models**  
Thiry and Guth [12] suggest classification-denoising networks, which simultaneously model image classification and denoising by learning a single network that holds the common distribution of noisy image information and their labels. Their method combines loss of cross-entropy classification with the proper denoising outcome at multiple noise levels, using the Tweedie–Miyasawa formula to estimate the denoised product. Experimental results in CIFAR-10 and ImageNet demonstrate competitive performance and improved adversarial robustness compared to standard discriminative classifiers. This study provides a theoretical link between denoising objectives and adversarial gradients, offering a new view of robustness that complements conventional defense mechanisms [12].
- **Reliable Robustness Evaluation**  
Croce and Hein [3] propose a robust evaluation framework for adversarial robustness based on a crew of various parameter-free attacks. Unlike earlier benchmarks that often build on individual attack procedures, Their ensemble joins complementary attacks such as APGD and Square attacks to provide a parameter-independent and safe robustness rating. The evaluation of the study was tested on more than fifty models and explained that many Already considered robust defenses could be broken when value with the suggested attack ensemble. This study highlighted the need for strict and united robustness estimate in adversarial machine learning and directly Motivated the use of AutoAttack as a reliable benchmark in the current work.

### 3. Materials and Methods

To develop a robust and adversarial classifier, a structured sequence of fundamental phases is required for the proper implementation of a machine learning model. In this work, a neural network-based model is adopted as the core classification algorithm. The proposed classifier is constructed through four main stages, each comprising a set of well-defined sub-processes prepared to ensure computational correctness, stability, and robustness against adversarial attack. These four stages are shown in Figure 1.

#### 3.1. Preprocessing data set

The data set was selected from Kaggle, a well-known platform for data science and machine learning research. This data set contains brain magnetic resonance images with identical segmentation masks, which are usually used to train and evaluate brain tumor segmentation models [13]. This data set consists of approximately 2,200 brain magnetic resonance images, each with a binary segmentation mask that highlights the tumor part at the pixel level. It is intended for semantic segmentation function and has been mostly used in research and public notebooks on Kaggle to train and evaluate deep

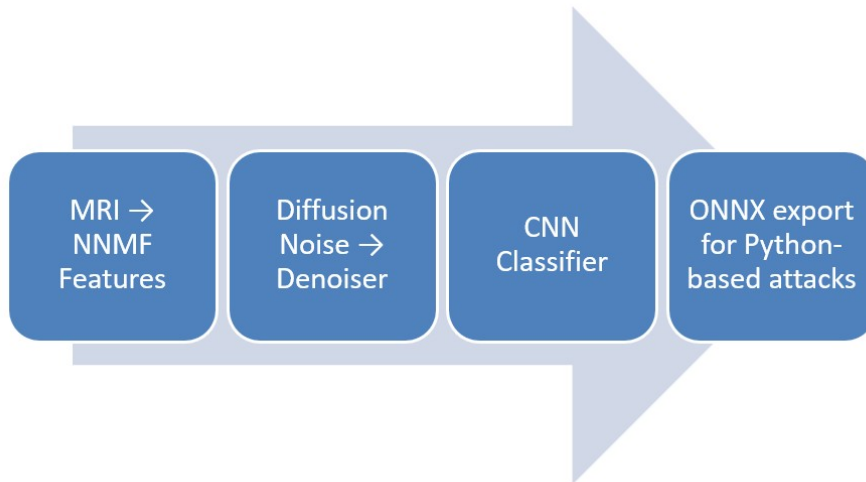


**Figure 1.** Stages of the proposed framework

learning models such as U-Net and its variants for brain tumor analysis. It was originally provided in the "COCO annotation" format, where the images and their corresponding labels were stored separately in a JSON file. The first preprocessing script in Python was developed to reorganize the data set into a folder directory structure suitable for image classification tasks. The script parses the annotation file, maps each image to its corresponding category, and saves the images to dedicated folders that represent each class: 730 training, 219 validating and 97 testing items for normal images, and 770 training, 210 validating and 118 testing items for tumor images. Thus, the train/validation/test ratios were kept and the single original Kaggle split was used only [13], i.e., 70%/20%/10%, resp. There was no exact information on the number of slices per patient, neither for the patient-wise representation. Because patient identifiers are not available, slice-level leakage between splits cannot be fully ruled out, and the reported performance may be optimistic compared to a strictly patient-wise evaluation. See details on the risk of slice-level leakage in brain magnetic resonance imaging classification in [14].

These preprocessing steps enable for smooth integration with convolutional neural network training.

### 3.2. Extraction Feature Phase Using NNMF

In this phase, features are extracted from each image using Non-Negative Matrix Factorization (NNMF). NNMF is a mechanism to factorize a non-negative matrix  $V \in \mathbb{R}_+^{K \times N}$  into two non-negative matrices  $W \in \mathbb{R}_+^{K \times R}$  and  $H \in \mathbb{R}_+^{R \times N}$ , so that their product approximates  $V$ , as reported in [15].

$$V = WH + E \quad (1)$$

where  $E \in \mathbb{R}^{K \times N}$  is the reconstruction error matrix. The matrices  $W$  and  $H$  are estimated by minimizing the cost function between  $V$  and  $WH$  as follows [15]:

$$W = \arg \min_W C(V | WH), \quad \text{for fixed } H \quad (2)$$

$$H = \arg \min_H C(V | WH), \quad \text{for fixed } W \quad (3)$$

where  $C(A | B)$  indicates a distance measurement between the matrices  $A$  and  $B$ . Various distance measures can be used, such as the Euclidean distance, the Kullback–Leibler divergence, the Itakura–Saito divergence, and  $\beta$ -divergence.

NNMF is used not only as a dimensionality-lowering mechanism, but also as an interpretable low-rank approximation model for non-negative data. As clarified in the SIAM study on Non-negative

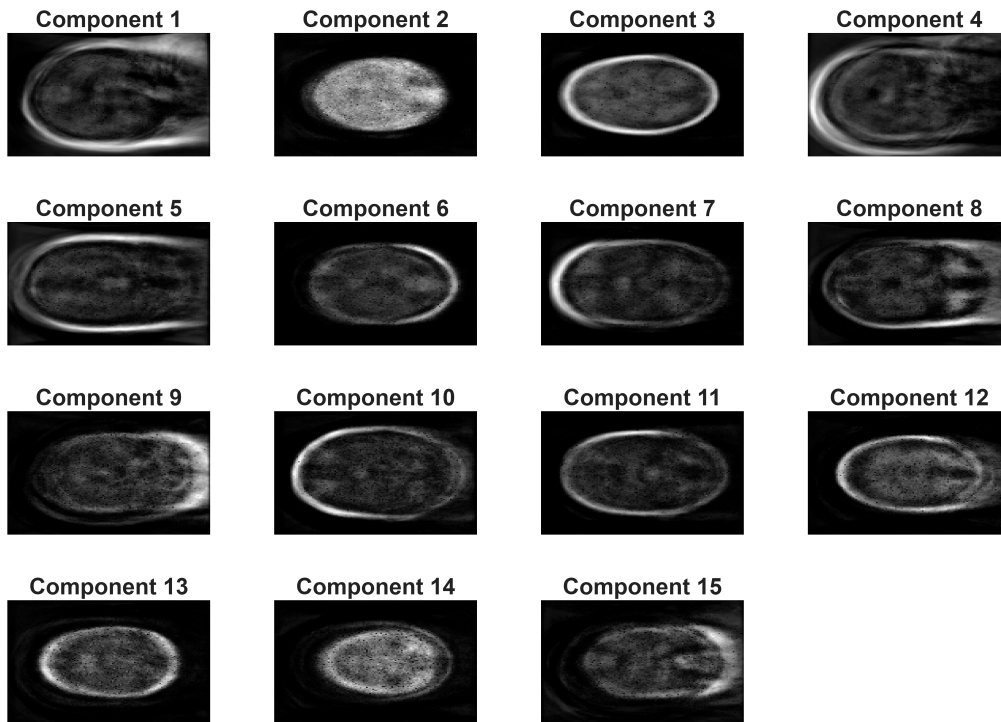


**Figure 2.** NNMF Basis Components ( $k = 15$ ). This figure shows the learned NNMF basis components got from the training data. Each basis image represents a non-negative spatial pattern that contributes to rebuilding brain MRI images. The components take meaningful anatomical structures such as skull boundaries, tissue distribution, and localized density variations. The variety across components indicates that NNMF decomposes the images into multiple complementary patterns rather than a single dominant structure, providing an interpretable and compact representation suitable for later analysis.

Matrix Factorization [7], NMF belongs to the family of linear dimensionality lowering mechanism, where every sample appears as an additive group of a small number of basis components under non-negativity chain's. Unlike PCA or unconstrained low-rank approximations, the non-negativity constraint executes parts-based representations, which are particularly proper for image analysis and medical data where pixel density is inherently non-negative.

Moreover, the option of an objective function significantly affects the obtained decomposition and its statistical interpretation [7]. Consequently, in the suggested framework, NNMF is optimized using the Kullback–Leibler (KL) divergence with multiplicative update rules [16]:

$$W \leftarrow W \otimes \frac{(V ./ (WH)) H^T}{\mathbf{1}_{K \times N} H^T} \quad (4)$$

$$H \leftarrow H \otimes \frac{W^T (V ./ (WH))}{W^T \mathbf{1}_{K \times N}} \quad (5)$$

where  $\otimes$  and  $./$  denote element-wise multiplication and division, respectively, and  $\mathbf{1}_{K \times N}$  represents a matrix  $K \times N$  whose elements are all equal to one.

The images were loaded using MATLAB Datastore with labels class from folder names. The image was transformed to grayscale if necessary, resized to  $128 \times 128$ , normalized to the  $[0,1]$  range, and vectorized to form a non-negative data matrix  $V$ , where each column represents one image. NNMF was learned using the training set, producing a basis matrix  $W$  and a coefficient matrix  $H$ . Validation and test features were got by drop their vectors onto the fixed basis  $W$  via non-negative least squares. Finally, the feature vectors were L2-normalized and saved for classification and robustness. Figures 2- 6 explain the steps to apply this method:

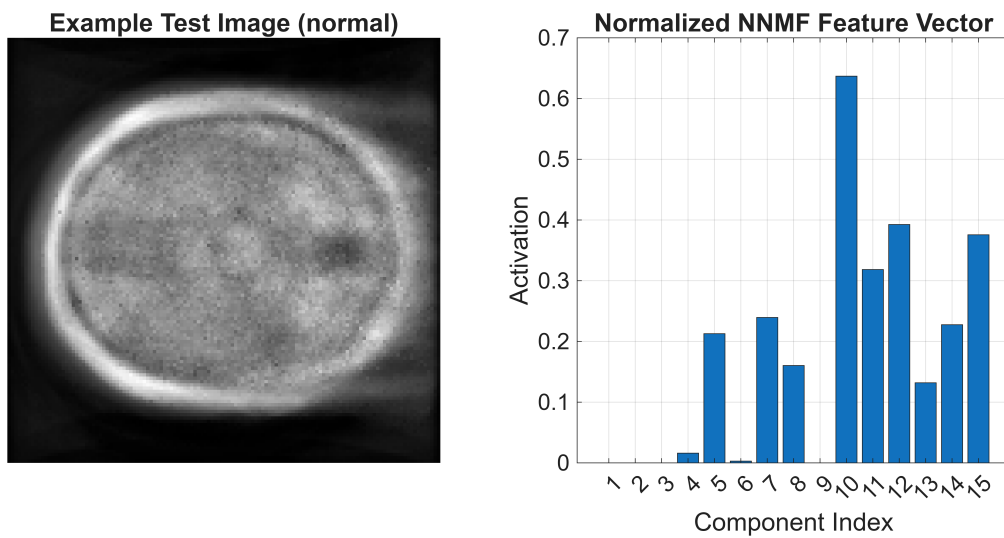


**Figure 3.** Example Test Image and Its Normalized NNMF Feature Vector. This figure illustrates an example test MRI image from the normal class side, its matching normalized NNMF feature vector. The bar plot shows the activation power of each NNMF component for this image, highlighting that only a subset of components exhibits strong responses. This sparse and selective activation pattern explains that NNMF features encode discriminative structural information rather than uniformly responding to all components, which is desirable for robust classification.

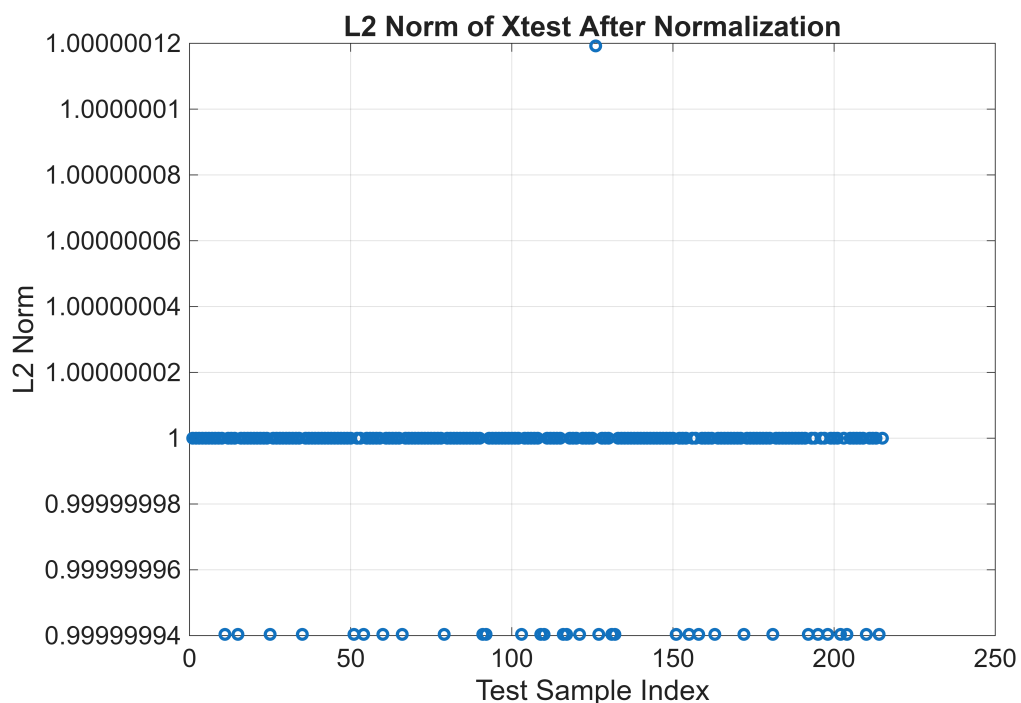


**Figure 4.** L2 Norm of Xtest After Normalization. This figure reports the L2 norm of all normalized test feature vectors. The values are tightly focused around one, confirming the right and stability of the normalization process. Ensuring unit-norm feature vectors is critical for fair comparison between samples and for robustness evaluation, as it blocks feature magnitude variations from controlling the classifier or adversarial attack.

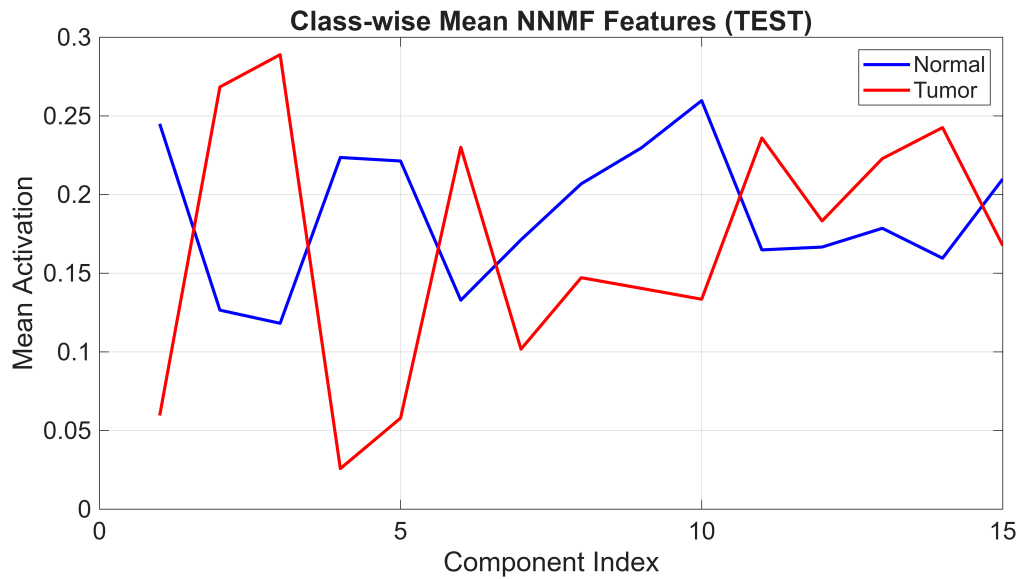


**Figure 5.** Class-wise Mean NNMF Features (Normalized, TEST). This figure shows the mean activation of each NNMF component for normal and tumor classes after feature normalization. Clearly, differences can be noticed via several components, where certain features show continuously, higher activation for tumor samples, while others are more prominent for normal samples. These class-dependent activation patterns indicate that NNMF components capture discriminative characteristics linked to pathological changes, supporting their effectiveness for classification and feature-space defense strategies.

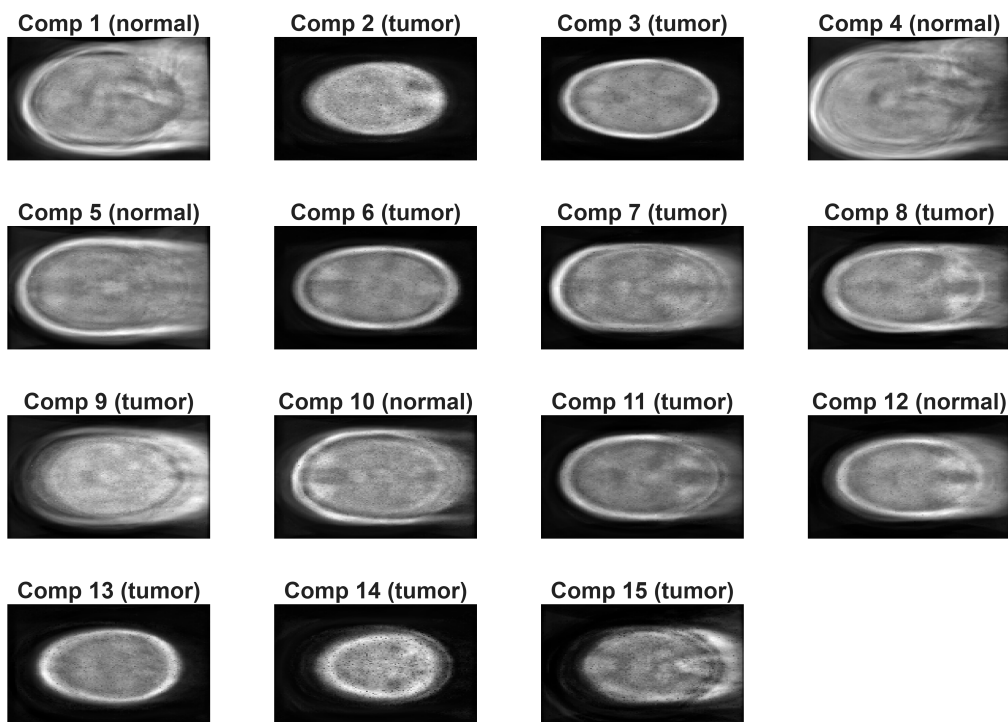


**Figure 6.** Top-Activated TEST Samples per Component (Using Normalized Xtest: This figure appears to be the most strongly activated test sample for each NNMF component based on normalized feature vectors. For each component, the corresponding image and its activation value are viewed along with the class label. The results detect that some components are often activated by tumour images, while others respond more strongly to normal brain structures. This component-wise association boosts interpretability by directly linking devoid feature dimensions to concrete visual patterns in MRI images

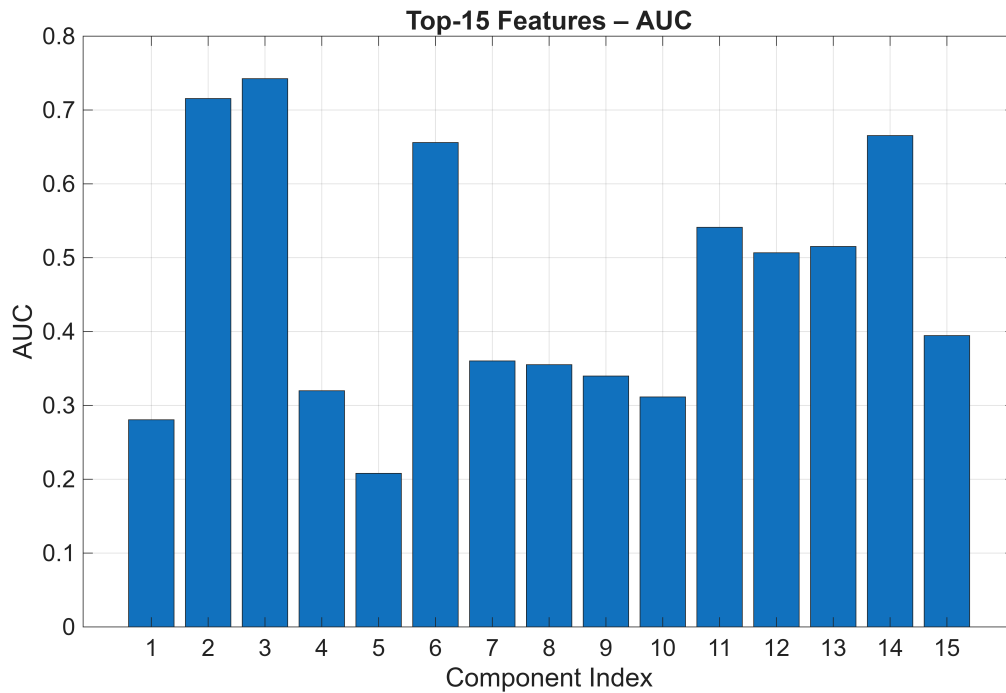


**Figure 7.** Top-15 Features – AUC. This figure shows the AUC rate of the top rate of NNMF features based on the feature selection operation. Each bar corresponds to a single NNMF component and affects its individual ability to distinguish tumor samples from normal ones. Higher AUC numbers indicate the most powerful discriminative ability, while values closer to 0.5 suggest limited separability. The score proves that several NNMF components show meaningful classification potential at the feature grade.

### 3.3. Feature Selection and Statistical Feature Analysis

Statistical analysis was performed on the NNMF features extracted from brain magnetic resonance images to identify the most distinguishing components to classify tumors and normal tissues, the NNMF rank was identified as 15. Each feature of the NNMF was individually evaluated using multiple complementary criteria, including the area under the ROC curve (AUC), the size of the effect measured by Cohen's d-value and the statistical significance assessed using Welch's t-test. This multi-criteria evaluation allows for an accurate result for the features by jointly considering discriminatory power, class separation size, and statistical reliability. The selected features provide interpretability and a concise representation suitable for subsequent classification and robustness analysis.

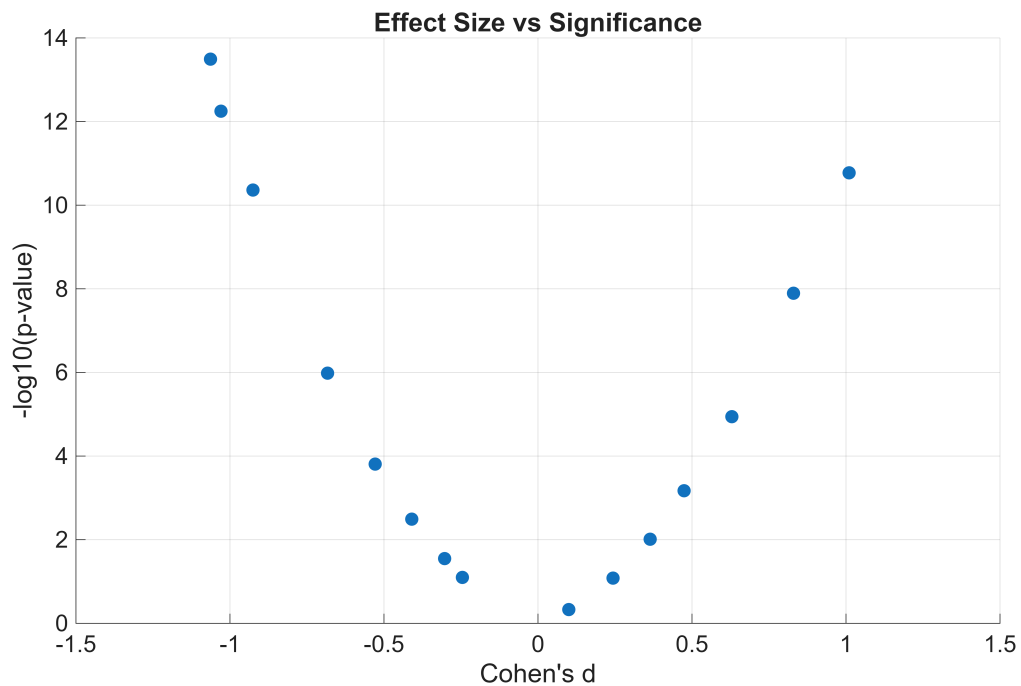


**Figure 8.** Effect Size vs Significance. This figure clarifies the relation between effect size and statistical significance for NNMF features. The horizontal axis marks Cohen's  $d$ , where positive values correspond to higher activation in tumor samples and negative values point to higher activation in normal samples. The vertical axis performs the negative logarithm of the  $p$ -value gained from Welch's  $t$ -test. Features with large absolute effect sizes and high statistical significance are visually stressed, highlighting components that are both hardly discriminative and statistically trusted.

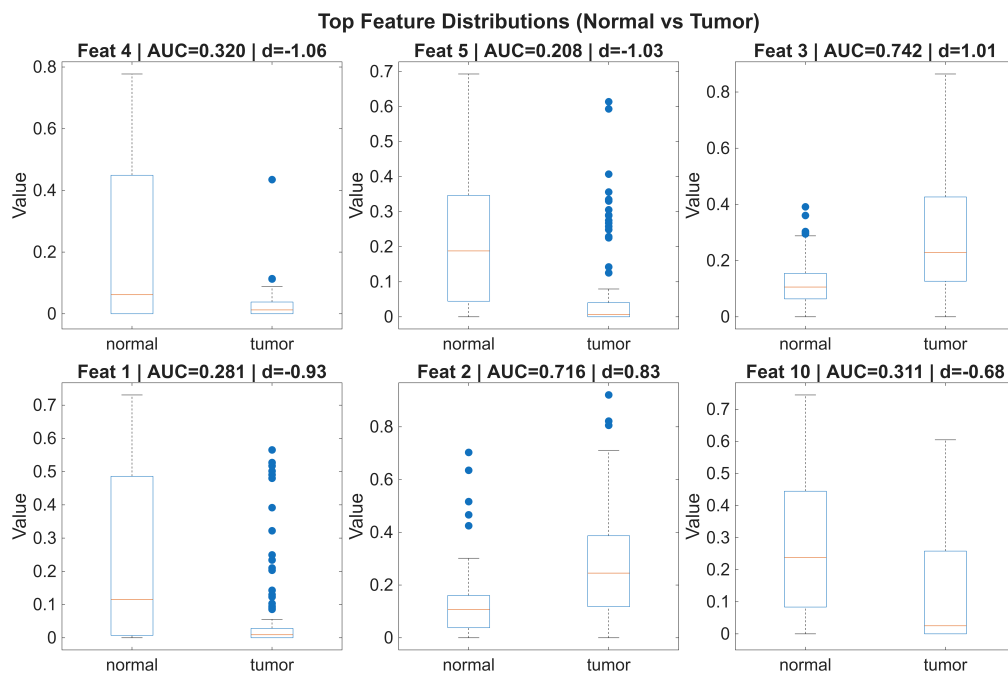


**Figure 9.** Top Feature Distributions (Normal vs Tumor) This figure displays boxplot visualizations of the maximum discriminative NNMF features, comparing their normalized distributions between normal and tumor classes. The plots detect visible differences in average and allocation spreads for selected features, providing visual confirmation of their discriminative stand. These distributions supplement the statistical metrics and explain how individual NNMF components react differently to healthy and sick brain structures.

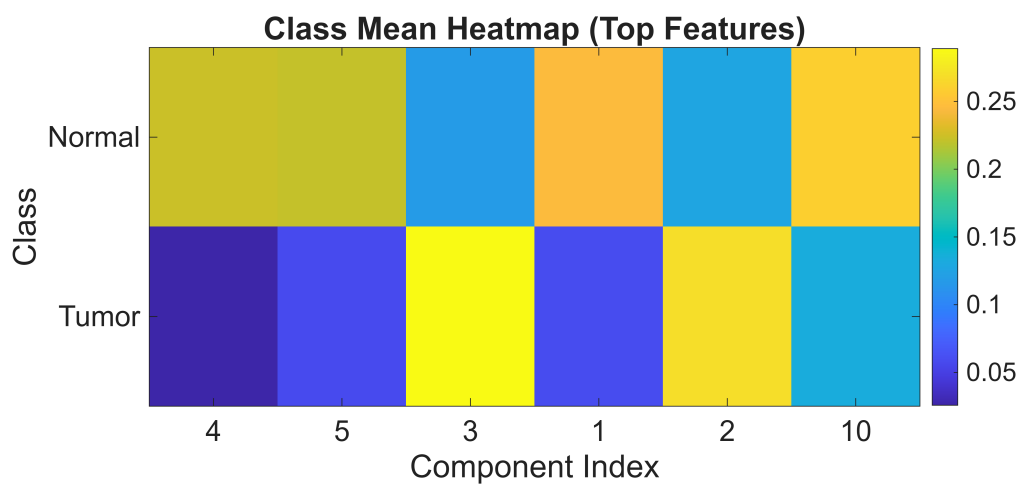


**Figure 10.** Class Mean Heatmap (Top-15 Features) This figure summarizes the class-wise mean activation of the top rate NNMF features using a heatmap representation. Every column reacts to a selected NNMF component, while rows represent the normal and tumor classes. The color intensity reflects the average feature activation, enabling speedily identification of tumor-dominant and normal-dominant features. The observed style confirms that NNMF components capture class-based structural information and contribute to interpretable feature-level discrimination.

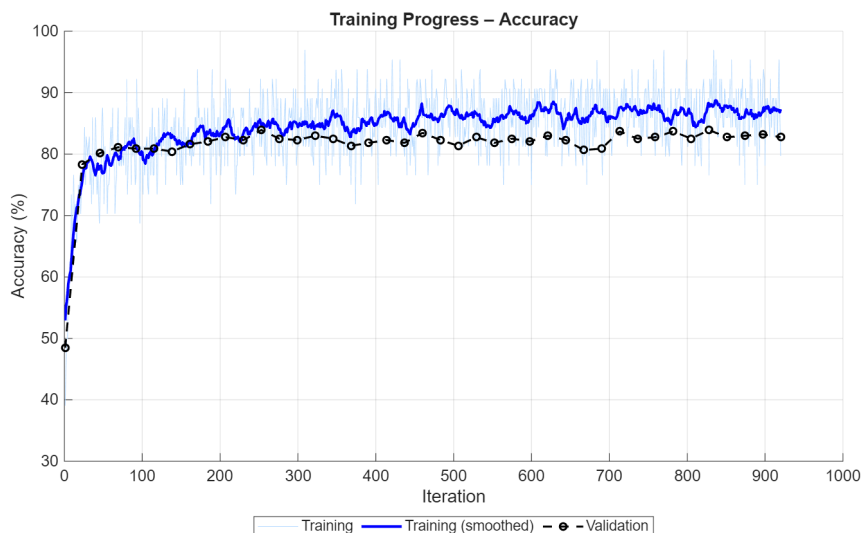


**Figure 11.** Training Progress – Accuracy This figure shows the evolution of classification accuracy via training. The light curve represents raw mini-boost training accuracy, while the smoothed curve highlights the total way. Validation accuracy (black markers) is measured periodically and close to the training curve, indicating stable learning and limited overfitting. Accuracy climbs sharply during the early iterations and then gradually saturates, proposing convergence of the model when trained on the selected NNMF feature space.

#### 3.4. CNN-Based Classification on Selected NNMF Features

After extracting features using NNMF, a statistical feature ranking stage is applied to evaluate the discriminative force of each NNMF component. Specifically, features are rated using multiple statistical criteria, including the Area Under the ROC Curve (AUC), Cohen’s effect size  $d$ , and  $p$ -values derived from hypothesis testing. These metrics quantify class separability and enable the selection of the most informative NNMF components while refusing redundant or weakly discriminatory features. Based on this ranking, a reduced subset of the top  $M$  NNMF features is selected and run as input to a lightweight Convolutional Neural Network (CNN) model. This step aims to explore whether the compact and interpretable NNMF representation is sufficient for proper brain tumor classification without the dependence on high-dimensional image inputs. before training, the selected feature vectors are smooth using L2 normalization per sample basis to stabilize the learning operation and ensure comparable feature scales across all samples. The CNN model is trained using the normalized NNMF features of the training set, while performance is monitored on a validation set to block overfitting. Lastly, the trained model ranks on a held-out test set using standard classification metrics, including accuracy and confusion matrices. This evaluation explains the effectiveness of combining the NNMF-based dimensionality decrease with CNN-based classification, achieving reliable tumor-versus-normal discrimination while maintaining a compact and strong feature representation. Similar hybrid NNMF-CNNs strategies have been shown to be effective in related style recognition and signal processing models, where NNMF supplies interpretable features and CNNs capture nonlinear decision boundaries [10,16].



**Figure 12.** Training Progress - Loss This figure reports the training and validation loss curves over iterations. The training loss reduces steadily, while the validation loss follows a similar downward trend with a slightly higher amount, which is expected. The parallel behaviour of both curves suggests that optimization is forward normally, and the model generalizes reasonably well. The large shows a big difference between training and validation loss, indicating that the CNN is not severely overfitting in spite of being trained for multiple epochs.

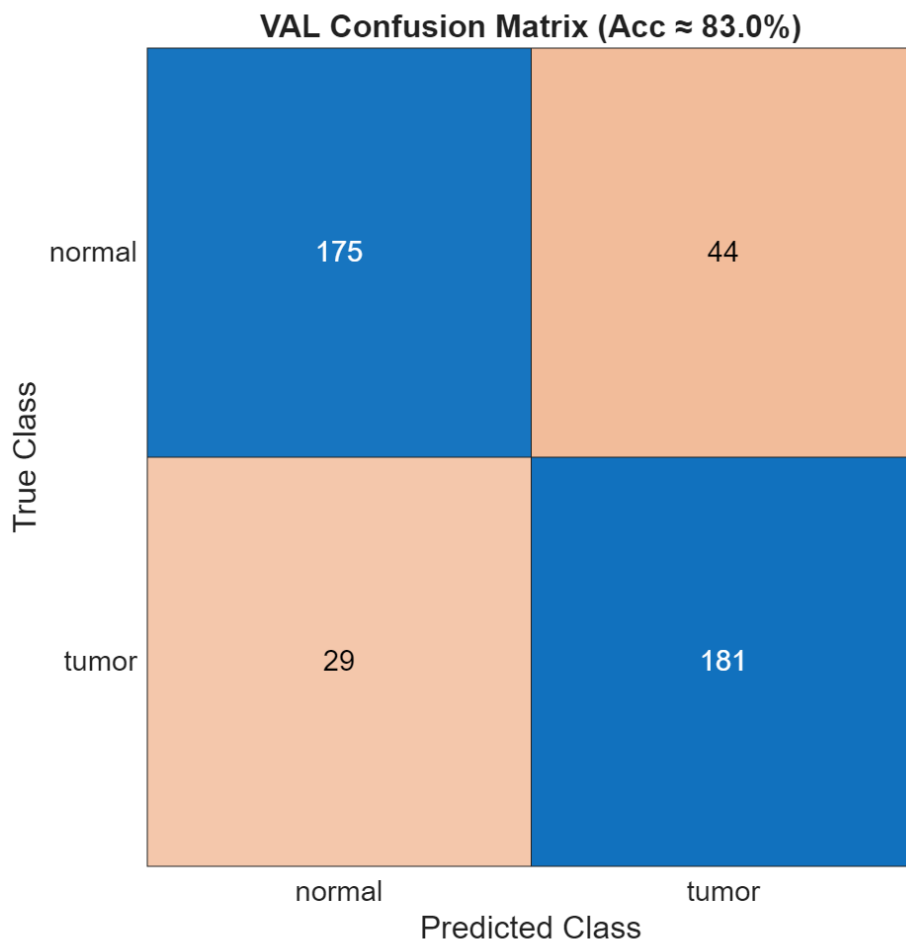


**Figure 13.** VAL Confusion Matrix (Acc  $\approx$  0.83). This confusion matrix abstract model's performance on the validation set. Correct predictions show on the diagonal, while off-diagonal input corresponds to wrong classifications. The matrix points a high rate of correctly classified normal and tumor samples, with errors basis occurring when normal images are predicted as tumor and vice versa. The total validation accuracy (83% confirms that the selected NNMF features retain meaningful discriminative information and that the classifier is learning a separable decision limit.

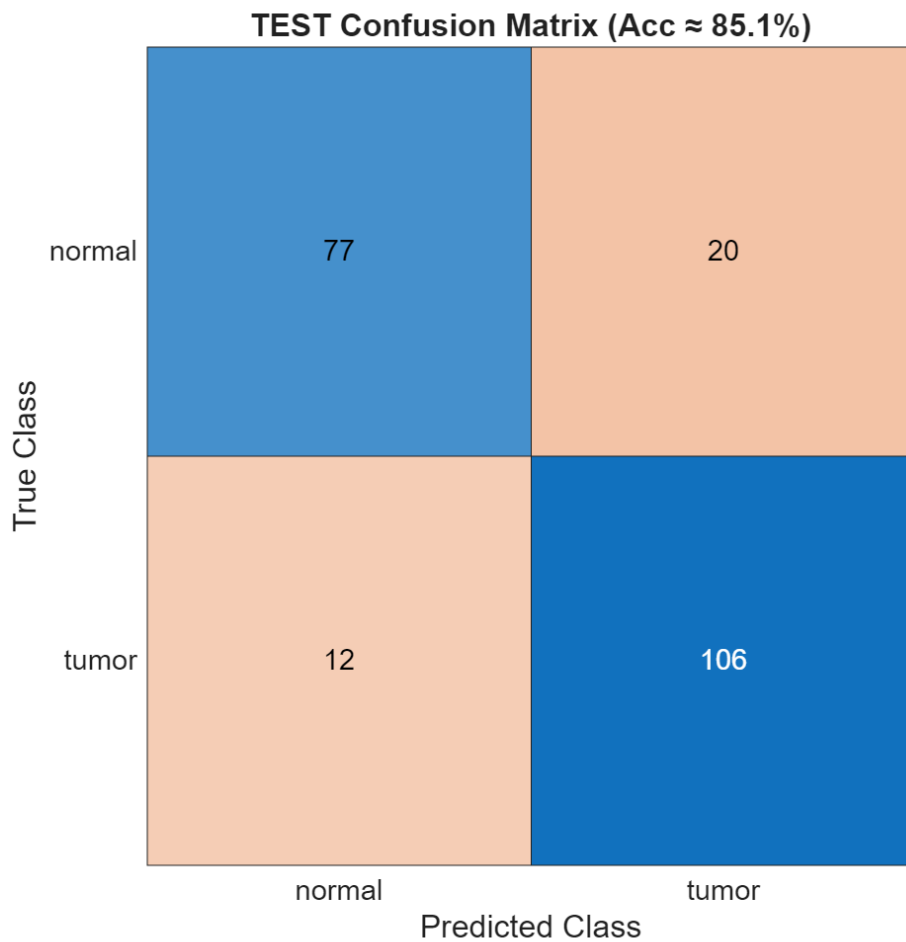


**Figure 14.** TEST Confusion Matrix (Acc  $\approx$  0.851). This confusion matrix reports final performance on the unseen test set. The majority of samples lie on the diagonal, return an overall accuracy  $\approx$  0.851. The relatively low number of false positives (normal  $\rightarrow$  tumor) and false negatives (tumor  $\rightarrow$  normal) points to balanced performance across both classes. This result supports the effectiveness of using a compact subset of NNMF features (selected by statistical ranking) as input to a small CNN, achieving robust generalization while reducing dimensionality.

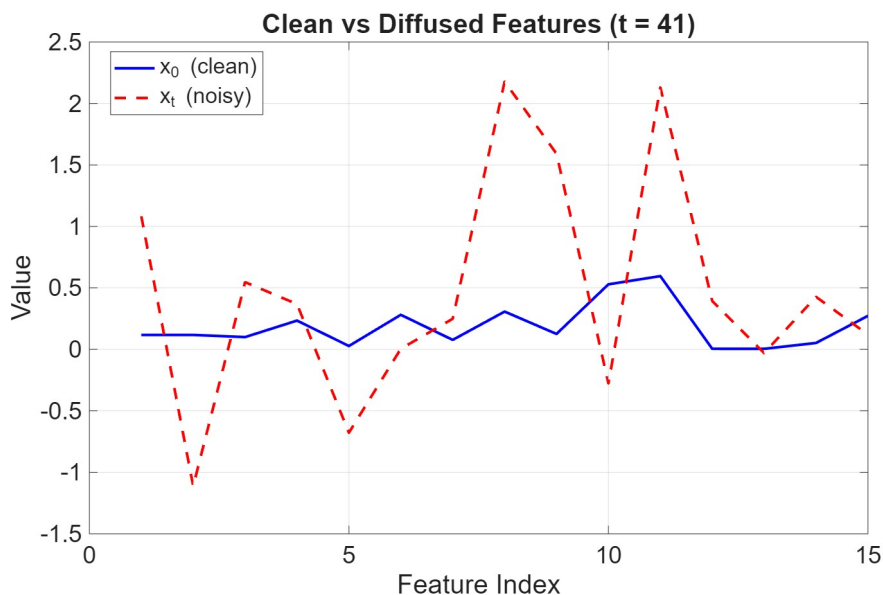


**Figure 15.** Clean vs diffused NNMF feature vectors at a late diffusion time step ( $t = 41$ ). The figure shows the impact of forward diffusion noise on selected feature components, view how the original clean features  $x_t, x_0$  are gradually corrupted to getting noisy features. trusted.

### 3.5. Feature-Space Diffusion Data Generation

In this step, diffusion training data was built in the NNMF feature space to allow feature-level denoising. First, the most discriminative Top-M NNMF features were selected based on the feature rating obtained from the labeling phase. All feature ranking statistics were computed exclusively on the training set; the selected Top-M components were then applied unchanged to the validation and test sets. To ensure consistency via the pipeline, the same per-sample L2 normalization used by the classifier was implemented for all selected features. A forward diffusion process was then defined using a linear noise timetable with a fixed number of diffusion steps. For each training sample, Gaussian noise was gradually added to the clean feature vector according to the accruing diffusion factor, generating noisy feature representations at randomly selected timesteps. This process resulted in paired samples consisting of clean features and noisy versions. The generated diffusion pairs were stored as  $(x_t, x_0)$ , where  $X_0$  indicates the original clean feature vector, and  $X_t$  represents its noisy counterpart in diffusion step  $t=41$ . These pairs form the training sets for the feature denoiser in the later step. In addition, the diffusion constants needed for inference and refinement were saved to ensure consistency between the MATLAB and Python implementations. This step does not involve model training or visualization; instead, it focuses only on setting up structured diffusion data that enables effective feature-space denoising and robust classification in subsequent stages. The figures below show the attitude of the NNMF features under the forward diffusion process, indicating the phased corruption of the feature representations as the diffusion time step increases.

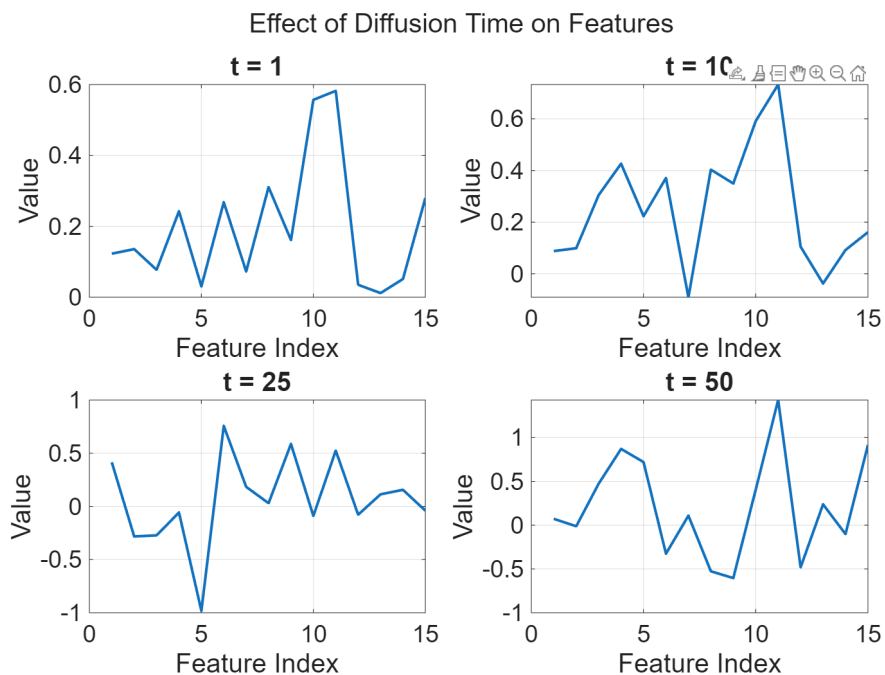


**Figure 16.** Impact of diffusion time on NNMF features at various timesteps ( $t = 1, 10, 25,$  and  $50$ ). As the diffusion timestep increases, the injected noise becomes more dominant, leading to higher distortion and variability in the feature representations.

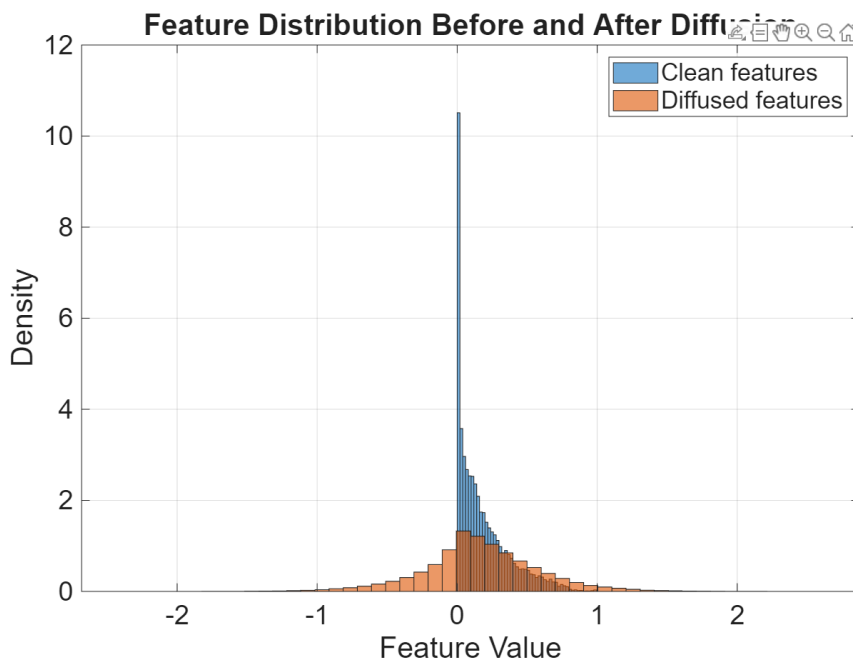


**Figure 17.** allocation of NNMF feature values before and after diffusion. The histogram comparison highlights the increase in contrast and spread of feature values caused by the diffusion operation, indicating a deviation from the original feature multiple.

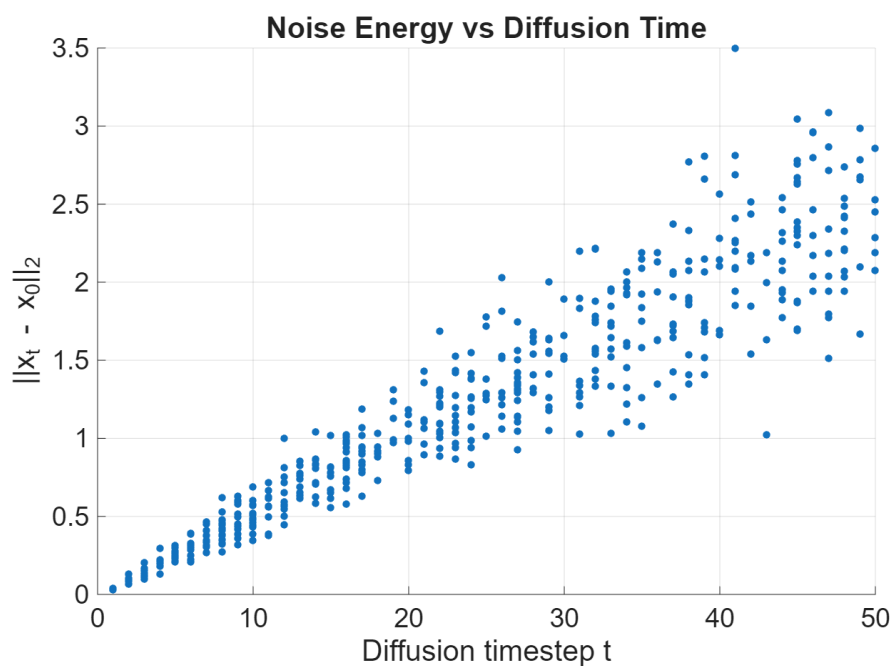


**Figure 18.** Noise energy as a function of diffusion timestep. The plot shows the L2 distance between clean and noisy feature vectors,  $x_t \|x_0$ , increasing with diffusion time, quantitative confirming the gradually damage introduced by the forward diffusion step.

Although the accumulative diffusion table is not explicitly explained, its effect is inherently reflected in the progressive rise of the noise capacity, which confirms how the contribution of the original clean features gradually reduces as the diffusion timestep boosts.

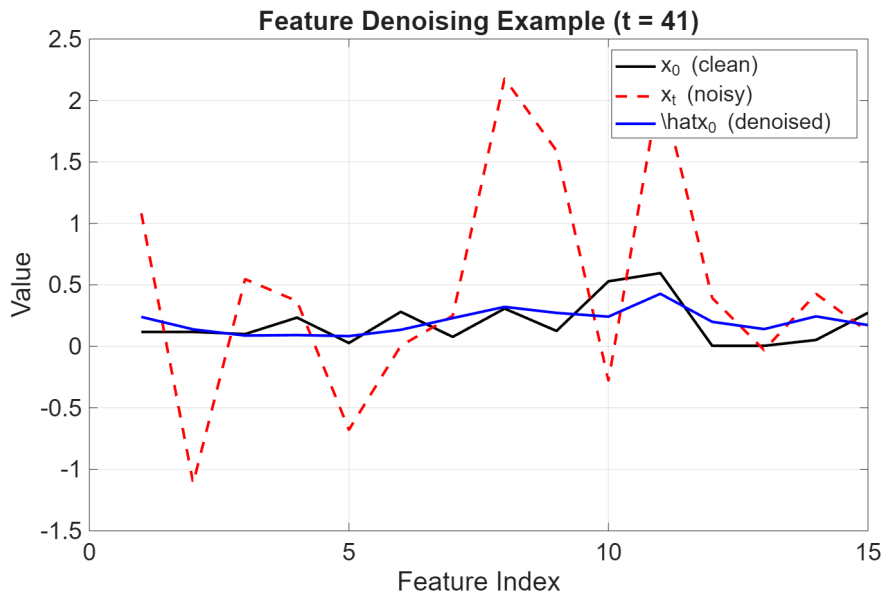


**Figure 19.** Feature denoising example at diffusion step  $t=41$ . The clean feature vector  $x_0$ , its diffused version  $x_t$ , and the denoiser output  $\hat{x}_0$  are drawn to explain how the network suppresses diffusion noise and movement, acting closer to the clean features.

### 3.6. Feature-Space Denoiser Training

After the construction of diffusion-corrupted feature pairs in the previous step, this stage focuses on learning a feature-level denoising model able to recover clean NNMF representations from noisy diffusion samples. The target of this step is to round the reverse diffusion step in the feature space by training a regression-based neural network that maps a noisy feature vector  $x_t$ , conditioned on its diffusion timestep  $t$ , back to its matching clean feature vector  $x_0$ . To allow for noise-level awareness, the diffusion timestep is coded using a compact sinusoidal embedding and hierarchically with the noisy feature input. The denoiser is optimized using a mean squared error objective, allowing it to gradually suppress diffusion-induced perturbations while keeping the underlying discriminative structure of the features. This trained denoiser serves as the basic component of the proposed diffusion-based defense, providing purified feature representations that are later used for robust classification.

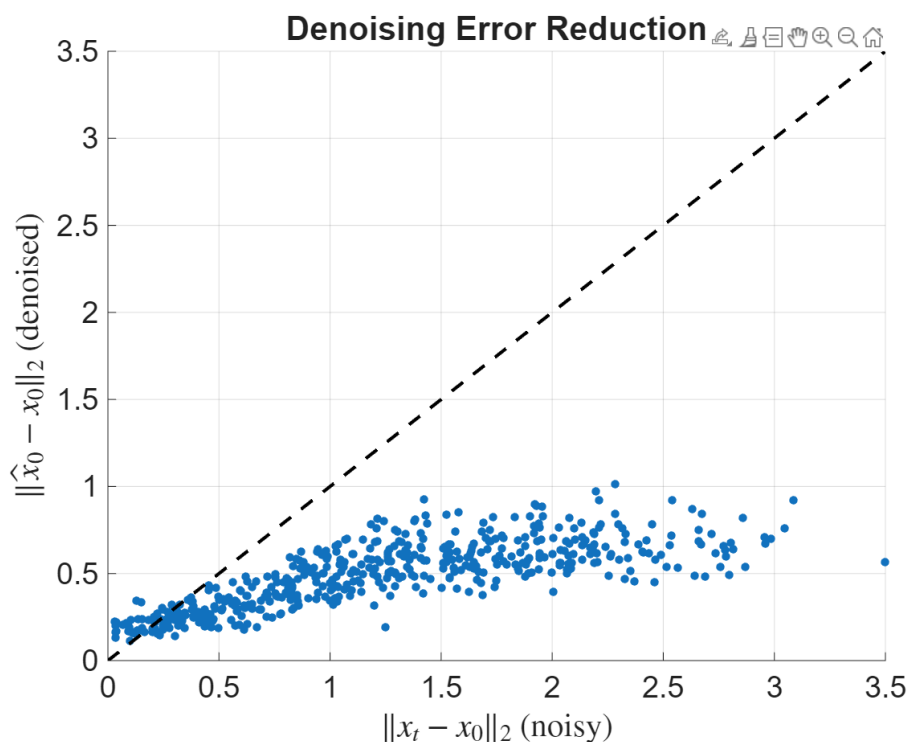


**Figure 20.** Denoising error is lowering relative to the noisy information. Each point contrast the noisy reconstruction error,  $\|x_t - x_0\|_2$  (x-axis), versus the denoised reconstruction error,  $\|\hat{x}_0 - x_0\|_2$  (y-axis). Points lying below the identity streak indicate successful fault decreases after denoising, demonstrating that the denoiser effectively returns features near the original clean representation.

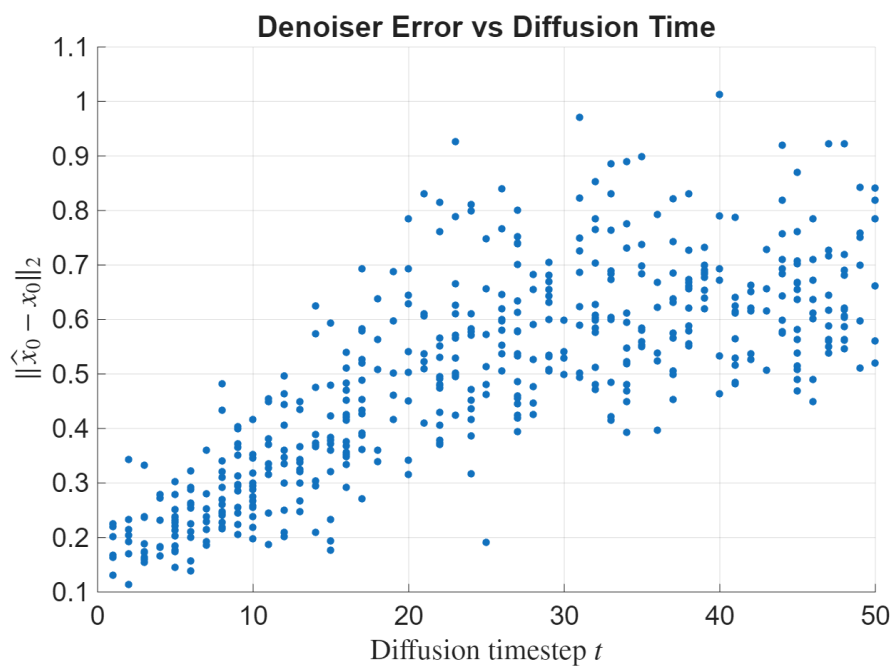


**Figure 21.** Denoiser reconstruction error versus diffusion time. The plot appears  $x_0\|_2\|\hat{x}_0$  as a function of timestep  $t$ , highlighting how denoising hard changes with increasing diffusion force.

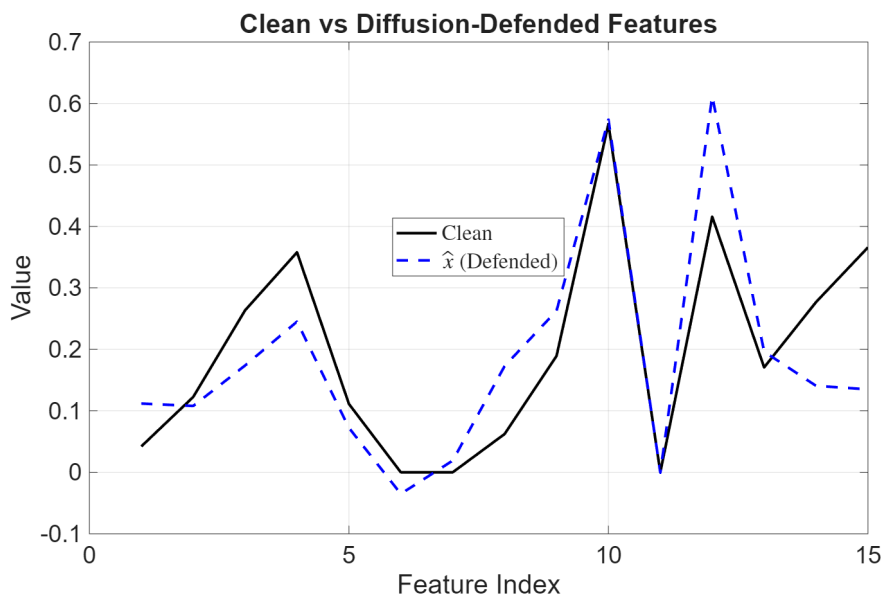


**Figure 22.** Clean vs. diffusion-defended NMF feature vector example on the test set, explain how the refine step alters the feature profile after forward noise and denoising at purt .

### 3.7. Evaluation of Feature-Space Diffusion refine

In this stage, we evaluate the suggested feature-space diffusion defense at the test time. The method implemented a forward diffusion step to perturb the clean NMF feature vectors at a chosen timestep purt, then used the trained denoiser to assess the clean features  $x_0$ . Finally, we compare the classifier performance on clean vs purified (defended) features using confusion matrices and test accuracy, and export a Python-ready defended test bundle for AutoAttack. The following data tables report types and quantitative comparisons between clean and diffusion-defended test features.

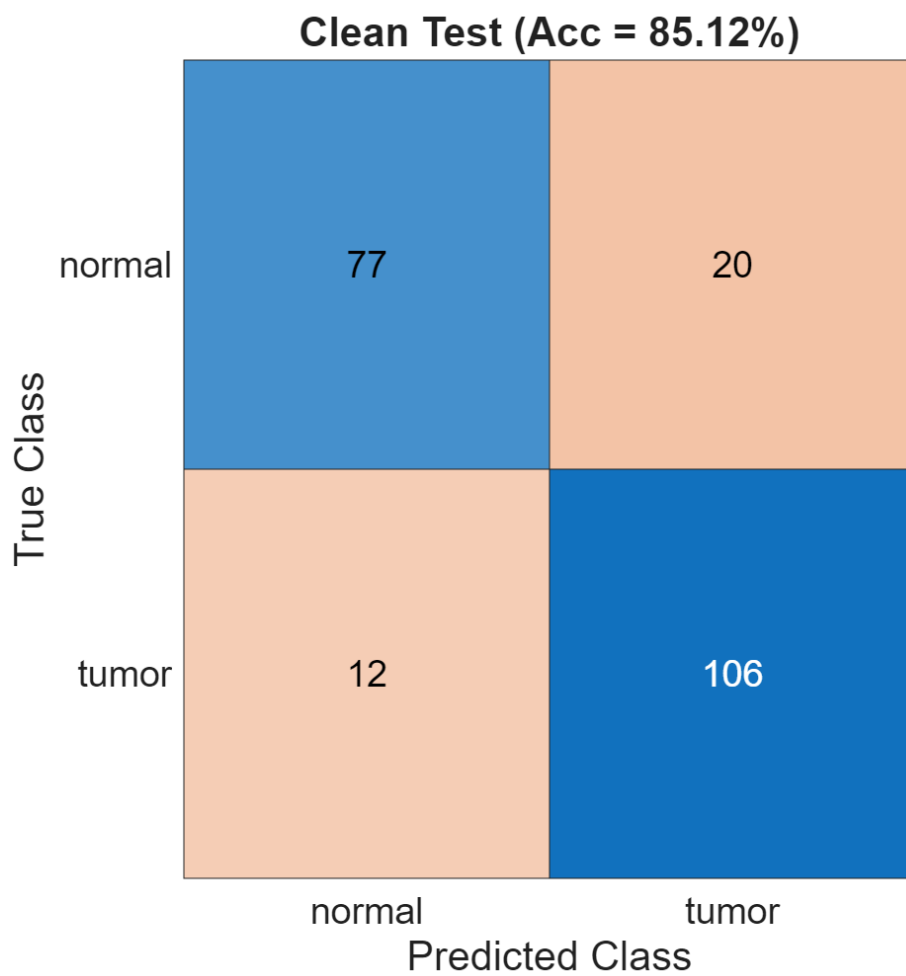


**Figure 23.** Confusion matrix on the test set using clean (non-defended) NNMF features, displays class-wise predicate outcomes for normal and tumor.

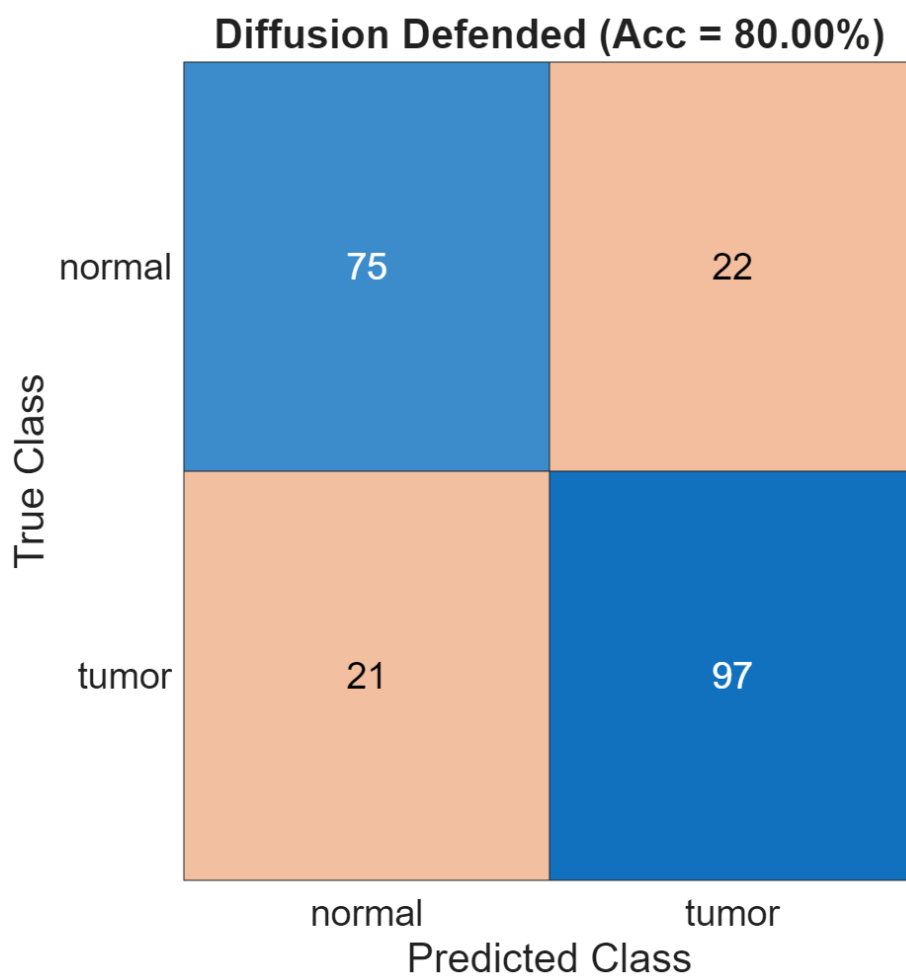


**Figure 24.** Confusion matrix on the test set after implementation of diffusion-based feature refinement (defended features), highlighting changes in misclassification patterns compared to the clean state.

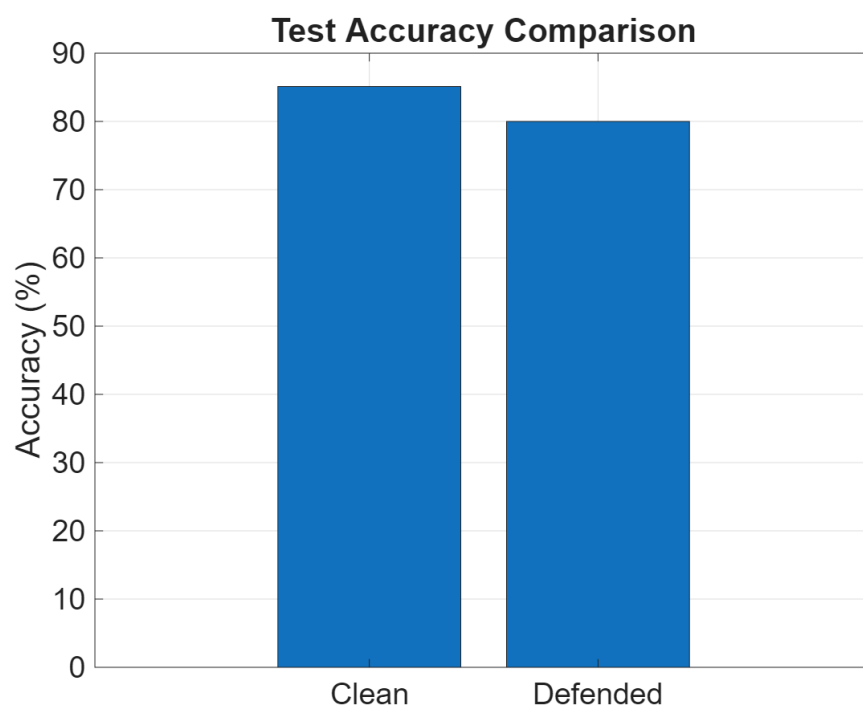


**Figure 25.** Test accuracy comparison between clean features and diffusion-defended (refine) features, quantifying the net effect of the defense on standard classification accuracy.

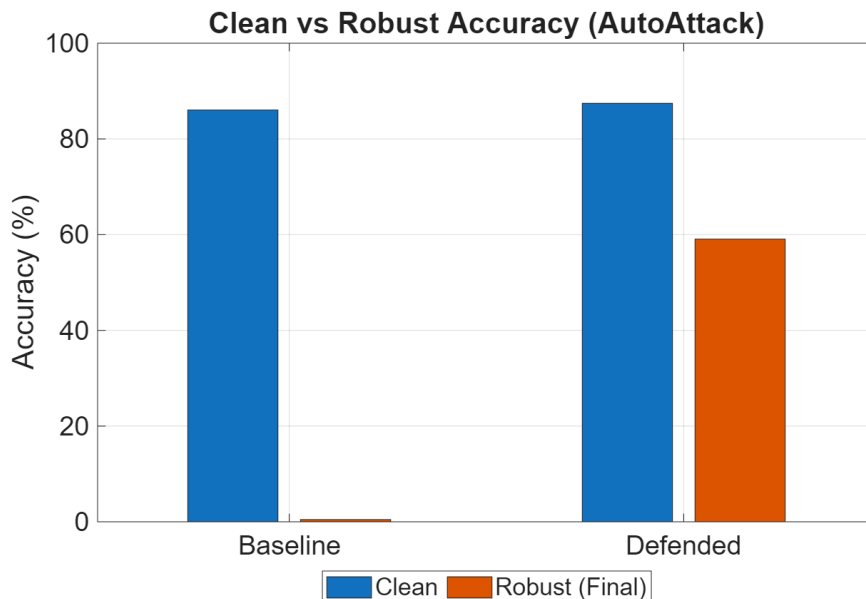


**Figure 26.** Clean and robust accuracy under AutoAttack ( $L_\infty$ ,  $\epsilon = 0.10$ ) for the clean model and the suggested diffusion-based defense. The robust accuracy corresponds to the final AutoAttack score (minimum across the evaluated attacks).

### 3.8. Robustness Evaluation under AutoAttack

In this stage, we evaluate the robustness of the suggested diffusion-based feature defense under robust adversarial attacks. We run AutoAttack ( $L_\infty$ ,  $\epsilon = 0.10$ ) using two components (APGD-CE and Square) on both the clean classifier and the defended pipeline (forward diffusion noise + feature denoiser + classifier). Since defense is random due to injected noise, Expectation over Transformation (EOT) is applied by medium predictions over multiple random samples ( $K=8$ ). The robustness is according to the attack and as the final robust accuracy.

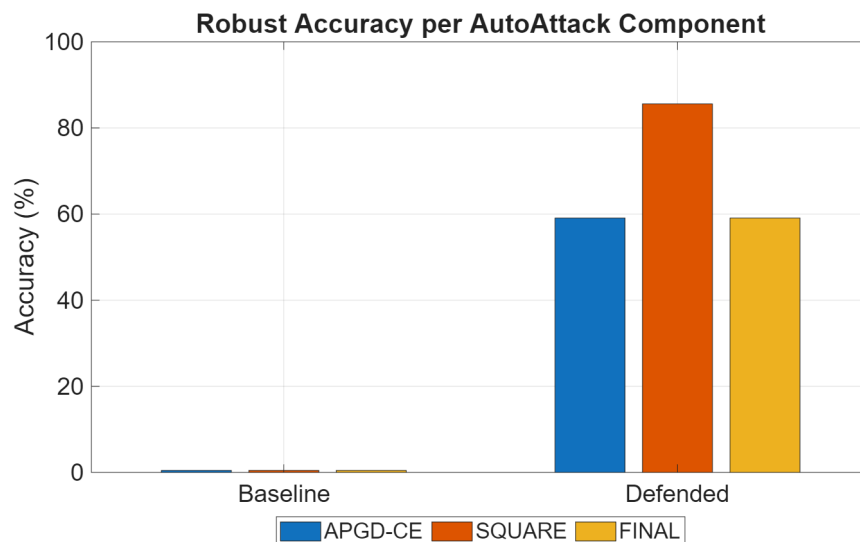


**Figure 27.** Robust accuracy per AutoAttack component (APGD-CE and Square) for the baseline and defended models ( $L_\infty$ ,  $\epsilon = 0.10$ ). The final robustness is calculated as the minimum accuracy across attacks.

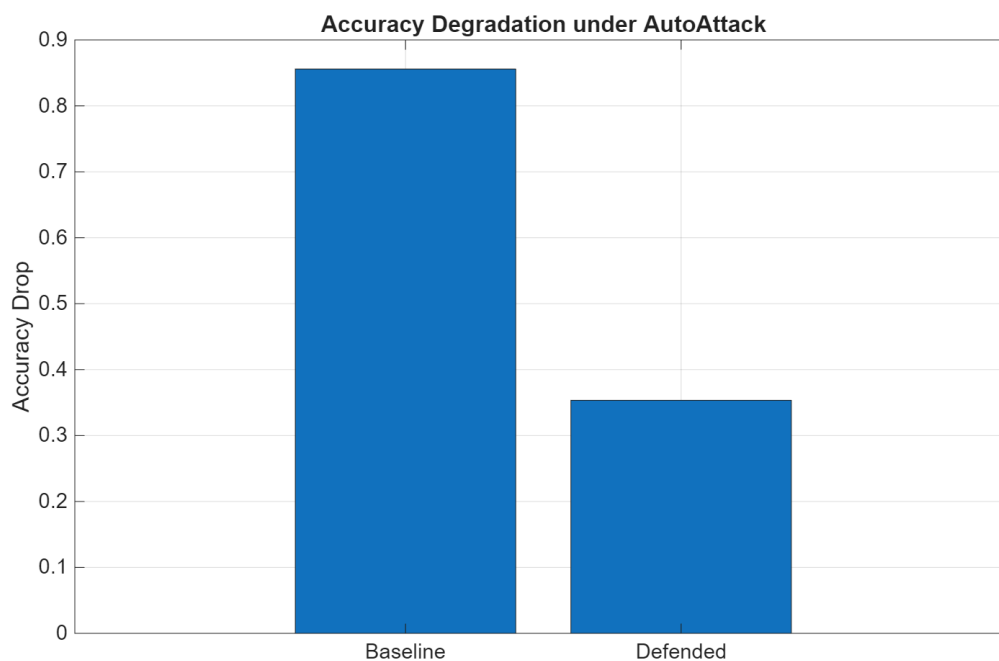


**Figure 28.** Accuracy decline under AutoAttack for baseline versus defended models ( $L_\infty$ ,  $\epsilon=0.10$ ). The diffusion-based defense noticeably reduces the drop from clean to robust performance.

### 3.9. Comprehensive Performance Evaluation

In addition to classical classification metrics, a total probabilistic rating was performed to estimate discrimination capacity and probability standardization under clean and adversarial conditions. Inspired by practical discussions on metric selection in the classification system [17], We used ROC-AUC, Brier score and Log-Loss, along with precision, Recall, F1-score, Matthews Correlation Coefficient (MCC) and balanced precision.

#### 3.9.1. ROC-AUC

The Receiver Operating Characteristic Area Under Curve Measurement (ROC-AUC) measures how well the pattern states positive samples above negative samples, independently of a fixed classification threshold [17]. A higher ROC-AUC indicates a powerful discrimination ability.

#### 3.9.2. Brier Score

The Brier score estimates the average squared error of the predicted probabilities:

$$\text{Brier Score} = \frac{1}{N} \sum_{i=1}^N (p_i - y_i)^2 \quad (4)$$

This metric can standardize the probability, where lower values indicate the highest probabilistic accuracy.

#### 3.9.3. Log-Loss

Log-Loss (cross-entropy loss) calculates the chance of predicted probabilities Given the true labels:

$$\text{LogLoss} = -\frac{1}{N} \sum_{i=1}^N [y_i \log(p_i) + (1 - y_i) \log(1 - p_i)] \quad (5)$$

Log-Loss with difficulty penalizes overconfident untrue predictions, making it useful and informative in adversarial tuning [17].

#### 3.9.4. Matthews Correlation Coefficient (MCC)

The Matthews Correlation Coefficient (MCC) is a stable performance metric that considers all values of the confusion matrix and is particularly suitable for unbalanced datasets. It is defined as:

$$\text{MCC} = \frac{TP \times TN - FP \times FN}{\sqrt{(TP + FP)(TP + FN)(TN + FP)(TN + FN)}} \quad (6)$$

where  $TP$ ,  $TN$ ,  $FP$ , and  $FN$  denote true positives, true negatives, false positives, and false negatives, respectively. The MCC amount ranges from  $-1$  (total disagreement) to  $+1$  (perfect prediction)

Balanced Accuracy was also included to relieve the possibility of class imbalance effects.

$$\text{Balanced Accuracy} = \frac{\text{Sensitivity} + \text{Specificity}}{2} \quad (7)$$

**Table 1.** Comprehensive Performance Comparison Under Clean and Adversarial Settings

Model	Acc	Prec	Rec	F1	MCC	BalAcc	ROC-AUC	Brier	LogLoss
Clean_Baseline	0.8605	0.8548	0.8983	0.8760	0.7178	0.8564	0.9105	0.1461	0.4751
Clean_Defended	0.8512	0.8525	0.8814	0.8667	0.6988	0.8479	0.8967	0.1555	0.4963
Robust_Baseline	0.0047	0.0000	0.0000	0.0000	-0.9906	0.0052	0.0075	0.4702	1.1629
Robust_Defended	0.5953	0.6115	0.7203	0.6615	0.1703	0.5818	0.7485	0.2150	0.6182

### 3.9.5. Results and Discussion

The results show that while the clean model suffers substantial degradation under adversarial attacks, the suggested diffusion-based defense preserves strong discriminative capability (ROC-AUC) and improved probability calibration (lower Brier Score and Log-Loss). These results support the importance of evaluating the classification model that employs discrimination and probabilistic metrics, as highlighted in [17]. The approx.  $-1$  of MCC under AutoAttack perturbations for the baseline indicates a complete reveal of the predictions and confirms that the adversarial attack effectively destroyed the classifier. Table 1 summarizes the quantitative comparison.

Figure 29 illustrates the comparative behavior of the evaluated metrics.

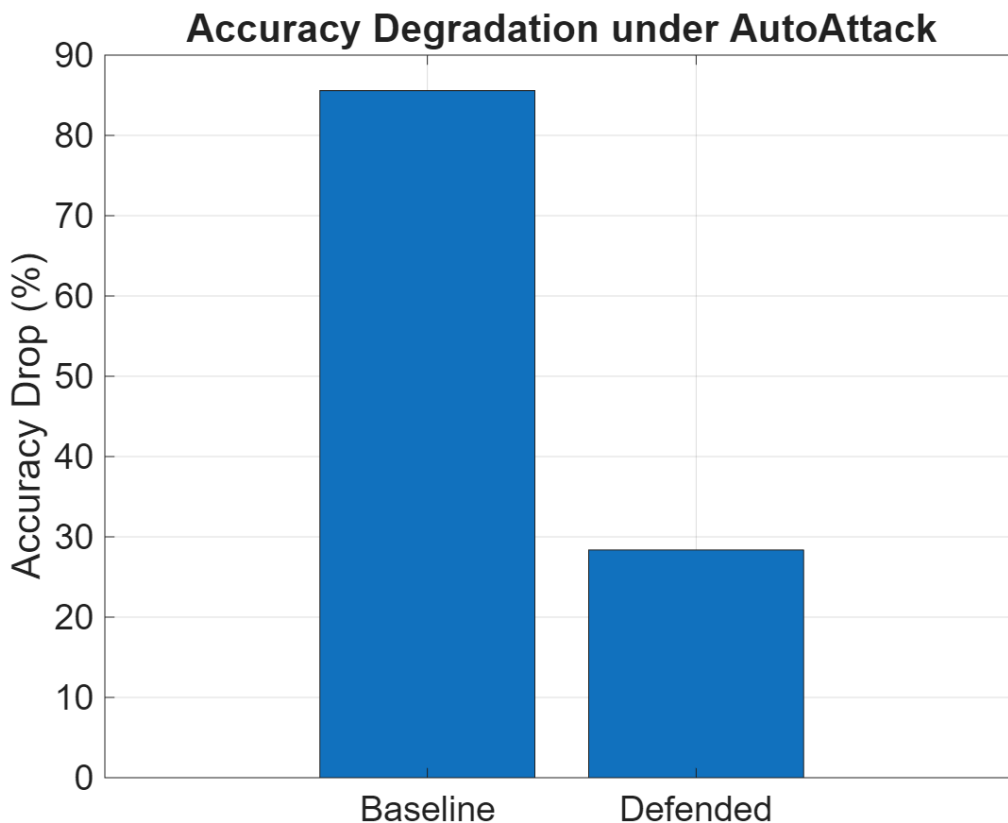


**Figure 29.** Comparison of classification and probabilistic metrics for baseline and diffusion-based defense under clean and adversarial settings. Higher values indicate better performance except for Brier Score and Log-Loss, where lower values are preferred.

**Table 2.** Execution Time Comparison (CPU vs GPU)

<b>Stage</b>	<b>CPU (sec)</b>	<b>GPU (sec)</b>
NNMF Feature Extraction	17.03	9.11
CNN Training (NNMF Features)	12.60	17.22
Diffusion Denoiser Training	8.42	9.24
AutoAttack Baseline (APGD-CE + Square)	8.42	10.73
AutoAttack Defended (APGD-CE + Square)	155.00	70.30
<b>Total Runtime</b>	<b>201.47</b>	<b>116.60</b>

## 4. Implementation and Computational Performance Analysis

The suggested framework was running using a combined MATLAB–Python pipeline. MATLAB was applied to NNMF for the extraction of features, statistical classification, CNN training, and a diffusion-based purification system. The trained models were exported to the ONNX format and run in Python using PyTorch and the AutoAttack framework for adversarial robustness rating.

All tests were carried out on a workstation armed with an Intel Core i7 CPU (16 GB RAM) and an NVIDIA RTX-series GPU with CUDA acceleration.

### 4.1. Computational Time Comparison

To analyse computational efficiency, we measured the execution time for all main phases of the suggested framework in both CPU and GPU environments. The results are summarized in Table 2.

#### *Analysis*

The results explain that GPU acceleration basically reduces the total runtime of the suggested framework. In special, the adversarial robustness estimate phase shows the most significant improvement, where the defended AutoAttack runtime minimizes from 155.00 seconds on CPU to 70.30 seconds on GPU, and there appears to be a major computational load.

The main differences are observed in lightweight stages, such as CNN training, due to GPU initialization and kernel beginning overhead. Since the NNMF feature volume is relatively small, the GPU does not provide a consistent advantage for all phases.

In general, GPU acceleration improves the overall runtime from 201.47 seconds to 116.60 seconds, obtaining approximately a speedup of 1.73× speedup. These results show that hardware acceleration is particularly useful for computationally strong adversarial robustness estimates, making the proposed framework practical feasible for large-scale analysis.

## 5. Conclusion

This study approaches a robust and structured framework for brain tumor classification based on NNMF feature extraction, statistical feature selection, CNN-based classification, and diffusion-based feature purity. Unlike a traditional end-to-end deep learning example that builds just on high-dimensional image input, the proposed path uses interpretable low-rank NNMF representations to build a compact and discriminative feature space.

The extracted NNMF components were statistically rated using metrics such as AUC, Cohen's  $d$ , and hypothesis testing, allowing the choice of the most informative features. A lightweight CNN classifier trained on the selected feature subset demonstrated competitive execution in clean test data while ensuring computational efficiency.

To direct adversarial vulnerability, a feature-space diffusion technique was applied, followed by a learned denoising model that approximates the reverse diffusion process. The robustness estimate under powerful adversarial attacks using AutoAttack guarantees that the proposed defense enhances stability compared to the baseline classifier. The experimental results show that combining interpretable NNMF features with diffusion-based purification improves adversarial robustness while maintaining classification accuracy.

In general, the suggested framework explains that the combination of statistical feature analysis, compact neural architectures, and a structured feature-level defense technique provides a stable solution between interpretability, accuracy, and robustness in the medical image classification model.

Future work may check the adaptive diffusion table, multi-step purity strategies, and extension to multi-class tumor levels tasks.

## 6. Acknowledgement

This work was supported by the Distinguished Professor Program of Óbuda University. The authors are also grateful for the possibility of using the HUN-REN Cloud <https://science-cloud.hu/en> [18] which helped us achieve some particular results published in this paper. Hiba Adil Al-kharsan gratefully acknowledges the financial support of the Stipendium Hungaricum Doctoral Program, managed by the Tempus Public Foundation.

1. Litjens, G.; Kooi, T.; Bejnordi, B.E.; Setio, A.A.A.; Ciomp, F.; Ghafoorian, M.; van der Laak, J.A.; van Ginneke, B.; Sánchez, C.I. A survey on deep learning in medical image analysis. *Medical Image Analysis* **2017**, *42*, 60–88. <https://doi.org/10.1016/j.media.2017.07.005>.
2. Szegedy, C.; Zaremba, W.; Sutskever, I.; Bruna, J.; Erhan, D.; Goodfellow, I.; Fergus, R. Intriguing properties of neural networks. 2013, International Conference on Learning Representations (ICLR) 2014. <https://doi.org/10.48550/arXiv.1312.6199>.
3. Croce, F.; Hein, M. Reliable evaluation of adversarial robustness with an ensemble of diverse parameter-free attacks. 2020, International Conference on Machine Learning (ICML) 2020. <https://doi.org/10.48550/arXiv.2003.01690>.
4. Guyon, I.; Elisseeff, A. An introduction to variable and feature selection. *Journal of Machine Learning Research* **2003**, *3*, 1157–1182. <http://www.jmlr.org/papers/volume3/guyon03a/guyon03a.pdf>.
5. Rajkó, R.; Siket, I.; Hegedűs, P.; Ferenc, R. Development of partial least squares regression with discriminant analysis for software bug prediction. *Heliyon* **2024**, *10*, e35045. <https://doi.org/10.1016/j.heliyon.2024.e35045>.
6. Lee, D.D.; Seung, H.S. Learning the parts of objects by non-negative matrix factorization. *Nature* **1999**, *401*, 788–791. <https://doi.org/10.1038/44565>.
7. Gillis, N. *Nonnegative Matrix Factorization*; SIAM, 2020. <https://doi.org/10.1137/1.9781611976410>.
8. Croce, F.; Hein, M. AutoAttack: Reliable evaluation of adversarial robustness. <https://github.com/fra31/auto-attack>, 2020. Last accessed: 10.03.2026.
9. Hossain, T.; Shishir, F.S.; Ashraf, M.; Al Nasim, M.A.; Shah, F.M. Brain tumor detection using Convolutional Neural Network. 2020, 1st International Conference on Advances in Science, Engineering and Robotics Technology (ICASERT-2019). <https://doi.org/10.1109/ICASERT.2019.8934561>.
10. Chan, T.K.; Chin, C.S.; Li, Y. Non-Negative Matrix Factorization-Convolutional Neural Network (NMF-CNN) for sound event detection. 2020, Detection and Classification of Acoustic Scenes and Events (DCASE) 2019 Challenge. <https://doi.org/10.48550/arXiv.2001.07874>.
11. Huang, H.; Yang, Z.; Liang, N.; Li, Z. Semi-NMF network for image classification. *IEEE Access* **2019**, *7*, 8899–8903. <https://doi.org/10.23919/ChiCC.2019.8866590>.
12. Thiry, L.; Guth, F. Classification-denoising networks, 2024. <https://doi.org/10.48550/arXiv.2410.03505>.
13. Darabi, P.K. Brain tumor image dataset: Semantic segmentation. <https://www.kaggle.com/datasets/pkdarabi/brain-tumor-image-dataset-semantic-segmentation>, 2023.
14. Yagis, E.; Atnafu, S.W.; García Seco de Herrera, A.; Marzi, C.; Sceda, R.; Giannelli, M.; Tessa, C.; Citi, L.; Diciotti, S. Effect of data leakage in brain MRI classification using 2D convolutional neural networks. *Scientific Reports* **2021**, *11*. <https://doi.org/10.1038/s41598-021-01681-w>.
15. Lee, S.; Pang, H.S. Feature extraction based on the Non-Negative Matrix Factorization of Convolutional Neural Networks for monitoring domestic activity with acoustic signals. *IEEE Access* **2020**, *8*, 122384–122395. <https://doi.org/10.1109/ACCESS.2020.3007199>.
16. Lee, D.D.; Seung, H.S. Algorithms for Non-negative Matrix Factorization. In Proceedings of the Advances in Neural Information Processing Systems. MIT Press, 2000, Vol. 13. [https://proceedings.neurips.cc/paper\\_files/paper/2000/file/f9d1152547c0bde01830b7e8bd60024c-Paper.pdf](https://proceedings.neurips.cc/paper_files/paper/2000/file/f9d1152547c0bde01830b7e8bd60024c-Paper.pdf).
17. Mazzanti, S. It took me 6 years to find the best metric for classification models. <https://medium.com/data-science-collective/it-took-me-6-years-to-find-the-best-metric-for-classification-models-0f5aa21a2b85>, 2023. Last accessed: 10.03.2026.
18. Héder, M.; Rigó, E.; Medgyesi, D.; Lovas, R.; Tenczer, S.; Török, F.; Farkas, A.; Emődi, M.; Kadlecsek, J.; Mező, G.; et al. The Past, Present and Future of the ELKH Cloud. *Információs Társadalom* **2022**, *22*, 128–137. <https://doi.org/10.22503/infars.xxii.2022.2.8>.